Displays 91 (2026) 103247

Contents lists available at ScienceDirect

Displays

journal homepage: www.elsevier.com/locate/displa

Chromatic waveguide near-eye display with stacked volume holographic gratings

Zhongwen Shen [a], Chao Ping Chen [b,*], Zhendong Wu [a], Dawei Zhu [a], Yan Yang [a]

[a] School of Electronic Information Engineering, Nanjing University of Industry Technology, Nanjing, China
[b] State Key Laboratory of Avionics Integration and Aviation System-of-Systems Synthesis, School of Integrated Circuits, Shanghai Jiao Tong University, Shanghai, China

ARTICLE INFO

Keywords:
Near-eye display
Waveguide
Volume holographic grating
Photopolymer

ABSTRACT

A chromatic waveguide near-eye display with wide-band stacked volume holographic gratings is proposed. The system parameters of holographic waveguide with one-dimensional exit pupil expansion configuration are systematically designed. The proposed stacked volume holographic gratings are successfully fabricated with color sensitive acrylate photopolymer and by varying exposure angles. Compared to multiplexed gratings, our stacked gratings can not only effectively increase the diffractive spectral bandwidths but also exhibit higher diffraction efficiency. To verify the imaging performance of the fabricated chromatic volume holographic waveguide, a full-color near-eye augmented reality display prototype, whose optical efficiency is 234.9 nit/lm, eye relief 18 mm, eye box 14 × 10 mm^2 and diagonal field of view 28°, is demonstrated.

1. Introduction

Volume holographic gratings (VHG) exhibits periodic refractive index modulation (RIM) in two-dimensional space, which allows the diffraction energy to be concentrated at specific diffraction order [1]. When incident light satisfies the Bragg diffraction conditions, VHG achieves exceptionally high diffraction efficiency. Meanwhile, diffraction efficiency would lead to a rapid decline when deviating from Bragg conditions [2]. Therefore, VHG exhibits excellent wavelength and angle selectivity, which makes it highly suitable for near-eye augmented reality (AR) displays [3].

Recently, holographic recording materials and VHG holographic waveguides are being extensively studied [4–14]. Holographic recording materials are crucial to the diffraction performance of VHG [15–17]. Silver halide and dichromated gelatin (DCG) were firstly used for holographic recording. Silver halide has a relatively broad diffraction bandwidth, typically ranging from 80 to 100 nm. However, its peak diffraction efficiency is only 30 %–40 %. On the other hand, VHG fabricated with DCG can achieve peak diffraction efficiency exceeding 90 %, and the relatively large diffractive wavelength bandwidth of 30 nm [18]. However, due to the sensitivity of gelatin to humidity, it must be encapsulated before use. In addition, holographic polymer dispersed liquid crystal (HPDLC) and photorefractive crystals were also studied for the fabrication of VHG holographic waveguide. Diao et al. (Changchun Institute of Optics, Fine Mechanics and Physics) investigated the holographic properties and electro-optic switch performance of HPDLC and successfully fabricated electrically controllable transmissive green VHG holographic waveguide [19]. However, due to the presence of numerous liquid crystal droplets, strong scattering occurs if the grating period is smaller than the liquid crystal droplet size. Odinokov et al. (Bauman Moscow State Technical University) fabricated a monochromatic green holographic waveguide with horizontal field of view (FOV) of 23° using photo-thermo-refractive glass [20]. However, increasing the number of multiplexes in the gratings is difficult to realize and the photorefractive glass requires baking at 500 °C after exposure [21]. In general, photopolymers are more suitable for fabricating holographic waveguide devices due to high refractive index modulation and good stability. Therefore, researchers have carried out extensive studies on VHG holographic waveguides with photopolymer, mainly focusing on expanding the FOV and realizing full-color display.

Currently, three types of holographic waveguide configurations are mainly proposed for achieving full color display: single-layer, double-layer, and three-layer [3]. In respect of single-layer VHG waveguide full-color displays, Kim et al. (Chungbuk National University) systematically analyzed the diffraction efficiencies of single-layer, double-layer, and three-layer color VHG structures prepared with Bayfol HX200 photopolymer [22,23]. In comparison, the double-layer stacked grating structure is the most balanced solution, with the highest diffraction

* Corresponding author.
E-mail address: ccp@sjtu.edu.cn (C.P. Chen).

https://doi.org/10.1016/j.displa.2025.103247
Received 4 July 2025; Received in revised form 25 September 2025; Accepted 28 September 2025
Available online 1 October 2025

efficiencies for red and green–blue composite VHGs. However, since the green and blue composite VHGs share the refractive index modulation of photopolymer, causing the diffraction efficiencies are only around 40 %. Mukawa et al. (Sony Corporation) proposed a double-layer chromatic holographic waveguide consisting of red-blue stacked VHGs and single layer green VHGs [4]. Compared with single-layer waveguide with color composite gratings, this solution cannot only ensure a high diffraction efficiency of over 70 %, but also avoid crosstalk, achieving a full-color display with a 16° horizontal FOV. However, no further discussion was made to expand the FOV of the chromatic volume holographic waveguide. Wu et al. (Beijing Institute of Technology) also successfully fabricated chromatic holographic waveguide by changing the interference angles of 532 nm laser, employing a right-angle prism as the in-coupling element and reflective VHGs as the out-coupling element, effectively simplified the exposure optical path [24–26].

For expanding FOV, Yu et al. (Zhejiang University) proposed spatially periodic gradient VHG, successfully achieving a diagonal FOV of 20° for single-red display [27]. Han et al. (Beijing Institute of Technology) proposed a holographic waveguide optical design with a free-form surface as the collimator and in-coupling elements, reflective composite VHGs for out-coupling [28,29]. Chen et al. (Shanghai Jiao Tong University) proposed the near-eye displays with dual-channel, triple-channel, quad-channel and penta-channel diffractive waveguides for the metaverse, finally achieving diagonal FOV of 109° [30–34].

In general, the current VHG holographic waveguides cannot simultaneously achieve high-efficiency, large-FOV, full-color near-eye displays. To address this issue, this paper proposes three-layer RGB waveguides with the broadband double-layer stacked gratings. Compared with the traditional chromatic holographic waveguides, the proposed broadband double-layer grating structure can not only effectively expand the FOV but also ensure high diffraction efficiency.

Specifically, a three-layered chromatic holographic waveguide with one-dimensional (1D) exit pupil expansion (EPE) configuration is designed and fabricated with color sensitive acrylate-based photopolymer. The problem of narrow diffractive bandwidth for red and blue VHGs is addressed through stacked grating structure. Simultaneously, an experimental prototype of VHG holographic waveguide display is constructed, featuring liquid crystal on silicon (LCoS) projector as the micro-display, and chromatic holographic waveguide as the main components. The imaging capabilities of the system are demonstrated and tested, validating the usability of the proposed chromatic waveguide with stacked VHGs for full-color near-eye AR displays.

2. Design and fabrication of chromatic volume holographic waveguide

2.1. Geometrical design for 1D EPE configuration

For designing 1D EPE configuration, it is necessary to consider various parameters, such as FOV, entrance pupil P_{in}, in-coupling grating size $i_x \times i_y$, waveguide thickness d, light propagation angle, and out-coupling grating size $O_x \times O_y$. As shown in Fig. 1, if the entrance pupil P_{in} of micro-display is larger than the length of in-coupling grating i_x, light rays at certain angles may not be diffracted into the waveguide, leading to FOV missing. Since the diffraction efficiency of in-coupling grating is very high, when the length of in-coupling grating i_x is wider than entrance pupil P_{in}, some light rays may undergo secondary diffraction out of the grating, significantly reducing the overall efficiency. To ensure the EPE continuity, the entrance pupil P_{in} of micro-display needs to be wider than the propagation period of marginal FOV rays. Therefore, the maximum angle θ_{max} of the rays propagated in the waveguide on x-axis, the micro-display entrance pupil P_{in}, and the length of in-coupling grating i_x needs to satisfy the following formula:

$$d \times tan\theta_{max} \le P_{in} \le i_x \tag{1}$$

The propagation angle of light also needs to satisfy the total internal reflection. So, the minimum propagation angle θ_{min} on x-axis can be calculated by the formula.

$$\theta_{min} = 2\xi - \frac{xFOV}{2} \ge arcsin\frac{1}{n} \tag{2}$$

where $xFOV/2$ represents the semi-horizontal FOV of the micro-display, ξ represents grating slanted angle, and n is the refractive index of flat waveguide.

As shown in Fig. 1(b), the collimated light in the FOV on y-axis will separate, resulting in a reduction of the exit pupil size in the y-direction. As the propagation distance increases, the light at the y-directional edge of the FOV separates further, potentially causing the FOV loss on y-axis when the light reaches the region of the out-coupling grating. From Fig. 1, we can see that to ensure the vertical eye box, the width of in-coupling grating i_y must be large enough, and the distance p between the in-coupling and out-coupling gratings should be designed reasonably, as indicated by the following formula.

$$p + O_x = \frac{iy - O_y}{2} \times tan^{-1}\left(\frac{yFOV}{2}\right) \tag{3}$$

where $yFOV/2$ represents half FOV on y-axis, O_x is the length of out-

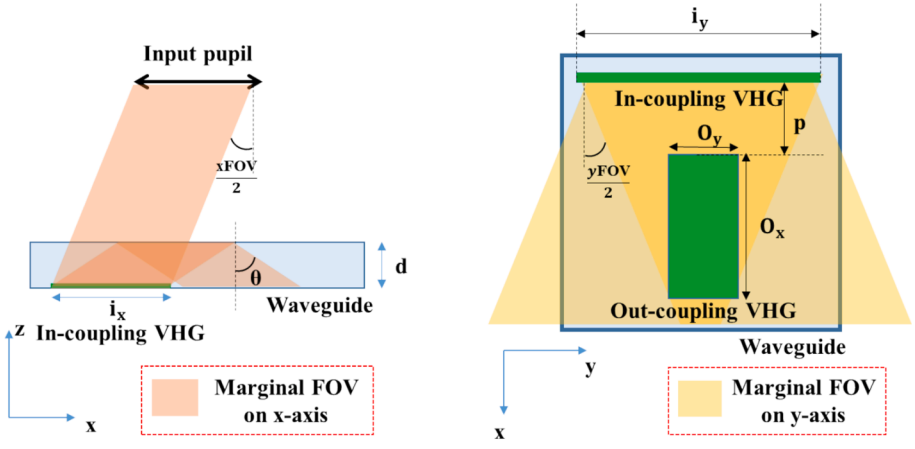

Fig. 1. Schematic of VHG holographic waveguide with 1D EPE configuration: (a) front view; (b) top view.

coupling grating.

As shown in Fig. 2, the width O_x and length O_y of out-coupling grating determines the eye relief (ER) and eye box size $xP_{out} \times yP_{out}$. Therefore, we need to design the length O_x, ER required for displaying the entire FOV, and size of eye box $xP_{out} \times yP_{out}$, which could be calculated by the following formula:

$$O_x = xP_{out} + 2ER \times tan\frac{xFOV}{2} \tag{4}$$

$$O_y = yP_{out} + 2ER \times tan\frac{yFOV}{2} \tag{5}$$

Thus, we finally designed the parameters of flat waveguide and coupling gratings for realizing diagonal FOV of 28° (24.4° × 13.9°), eye box of 14 × 10 mm^2, ER of 18 mm. The calculated parameters are presented in Table 1.

VHG exhibits strict diffraction wavelength and angle selectivity, resulting in a limited diffractive bandwidth [35–37]. This would limit the FOV of VHG holographic waveguide displays. Therefore, we initially investigated the diffraction efficiency distribution of VHG under different incident angles and wavelengths based on the designed parameters. Subsequently, considering the angle range covered by the spectral curve of micro-display, we assessed the FOV of the designed chromatic holographic waveguide.

2.2. Design for the coupling gratings parameters

The LCoS light engine used in this paper is developed by Lochn Optoelectronics Technology Co., Ltd., which can project image with a diagonal FOV of 28° (24.4° × 13.9°) in the air (display aspect ratio: 16:9). The exit pupil of the LCoS light engine is 6 mm × 20 mm, which is suitable for holographic waveguide with 1D EPE configuration. We have used fiber optic spectrometer (Qwave, RGB Photonics GmbH) to measure the LCoS projector spectrum. The measured RGB central wavelengths are 459.89 nm, 523.21 nm, and 623.02 nm, respectively. Fig. 3 illustrates the diffraction efficiency distributions of the designed RGB VHGs, the spectrums of the LCoS micro display is also added. Compared to the green VHGs, both red and blue VHGs cover relatively smaller area of the red and blue spectral bands of the LCoS light engine, requiring a stacked grating design to achieve full-field display in the horizontal direction. On the other hand, only one grating is needed for the green gratings to cover the display range of 24.4° in air, which corresponding to incident angle range of − 7.59° to 7.59° in the waveguide ($n = 1.6$). The in-coupling and out-coupling grating parameters need to be designed based on the spectrum of LCoS micro display, which are listed in Table 2.

Table 1
Geometrical parameters of holographic waveguides in x-y plane.

Object	Parameter	Value
In-coupling VHG	$i_x \times i_y$	6 mm × 20 mm
Out-coupling VHG	$O_x \times O_y$	22 mm × 14 mm
Waveguide	n	1.6
	d	1 mm
	p	15 mm

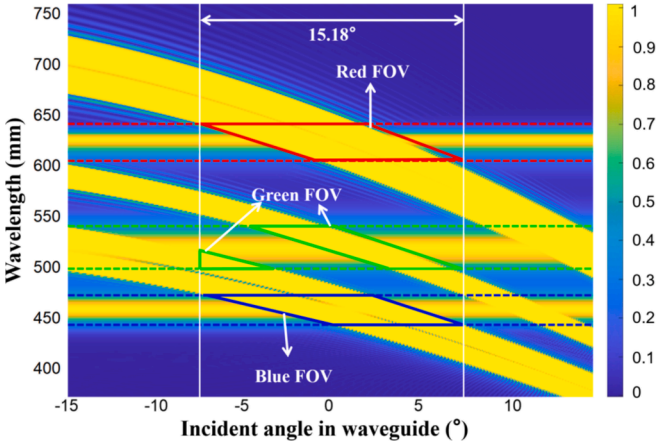

Fig. 3. Diffraction efficiency distributions of designed RGB VHGs and spectrum of LCoS light engine.

Table 2
Designed in-coupling and out-coupling grating parameters.

Object	Parameter	Value
In-/out-coupling VHGs	Central wavelength	R1: 600 nm; R2: 632 nm G: 523 nm B1: 450 nm; B2: 470 nm
	Grating period	Λ_{R1}: 228.1 nm; Λ_{R2}: 244.1 nm Λ_G: 198.9 nm Λ_{B1}: 172.8 nm; Λ_{B2}: 175.9 nm
	Grating slanted angle	30°

2.3. Fabrication of the designed VHGs

Multi-wavelength variable-angle exposure method is adopted to fabricate the designed RGB VHG holographic waveguides, respectively. The angle between the object light and reference light is determined by the recording and the reconstruction light wavelength. As shown in Fig. 4(a), when the reconstruction light wavelength is longer than the

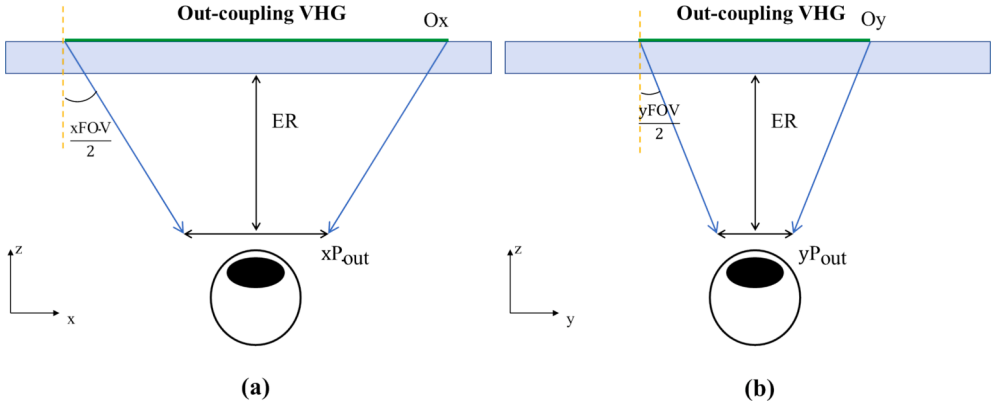

Fig. 2. Relationship among the FOV, size of out-coupling gratings, ER and eyebox: (a) front view; (b) side view.

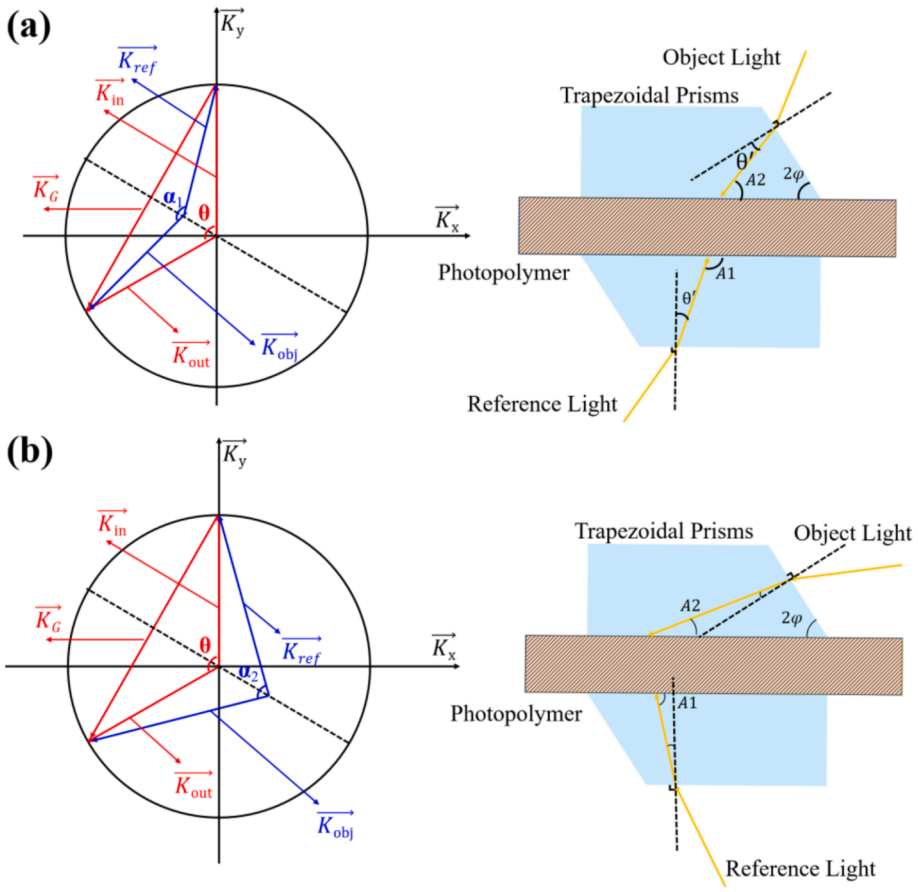

Fig. 4. *K*-vector diagrams for determining the exposure angles. (a) The *K*-vector of recording light is larger than that of reconstruction light. (b) The *K*-vector of recording light is smaller than that of reconstruction light.

recording light wavelength, the angle α_1 between the object light and reference light must be greater than the grating diffraction angle θ, which is twice the grating inclination angle 2φ. Conversely, if the reconstruction light wavelength is shorter than the recording light wavelength, the object-reference light angle α_2 must be smaller than the grating diffraction angle θ to fabricate the designed grating vector K_G. The object-reference light angle α can be calculated using the following formula:

$$\alpha = 2arcsin(\frac{\lambda_{record}}{\lambda_{reconstruction}} sin\frac{\theta}{2}) \tag{6}$$

Due to the large angle between the object light and the recording plane, a trapezoidal prism must be introduced to ensure that the reconstructed light satisfies the total internal reflection condition of the waveguide. As can be seen from the figure, the angles $\Delta\theta$ and θ' between the reference light/object light and the prism surface, the inclination angle φ of the trapezoidal prism, and the angle α between the object light and reference light must satisfy the following relationships:

$$\Delta\theta = \varphi - \frac{\alpha}{2} \tag{7}$$

$$\theta' = sin^{-1}(nsin(\Delta\theta)) \tag{8}$$

Based on the above formulas, we can separately calculate the recording light angles A_1 and A_2 corresponding to the designed red, green, and blue gratings. Fig. 5 shows the exposure method for the red and blue stacked VHGs and the green VHG. The optical setup for grating exposure is shown in Fig. 5(a). The single longitudinal mode solid-state lasers (MSL-FN-639, MSL-FN-532, MSL-FN-457, CNI) at 639 nm, 532 nm, and 457 nm were used as light sources. The laser is expanded and collimated with spatial filter (GCO-0112 M, Daheng Optics) and the double-glued achromatic lens (GCL-010615, Daheng Optics), with the expanded collimated light with 50 mm diameter. A polarization beam splitter prism (GCC-402103, Daheng Optics) is then used to divide the expanded collimated light into two beams. The intensity ratio and polarization state of the reference and object lights were adjusted by half-wave plates (GCL-0607, Daheng Optics), ensuring both are S-polarized. Finally, the interference angles of two beams were adjusted according to the data listed in Table 3 for sequential exposure. To reduce experimental complexity and errors, a mask is customized according to the waveguide design parameters in Section 2.1, which allows light to pass only through the grating area, enabling one-step fabrication of both the input and output coupling gratings.

As shown in Fig. 5(b), when fabricating the VHGs with large diffraction angle, the angle between the reference light and the recording plane is often much smaller than that of the object light. This leads to a significant difference on the beam intensity incident in the photopolymer. Therefore, to maximize the grating diffraction efficiency, the intensity ratio of the object-reference light for each grating should be calculated according to their interference angle, as shown in Table 3.

Additionally, this paper proposes three dyes sensitized method to prepare the color sensitive photopolymer, which utilize the polyvinyl acetate (PVAc) as the binder, n-vinylcarbazole (NVC), tetrahydrofuran acrylate (THFA), polyethylene glycol o-phenylphenyl ether acrylate (OPPEA) as the mixed monomers, 2,2′-Bis(2-chlorophenyl)-4,4′,5,5′-tetraphenyl-1,2′-biimidazole (BCIM) as the photoinitiator, aridine orange, algal red B and methylene blue as the photosensitizer. The preparation process is taken in the dark room (ambient temperature:25℃, relative humidity: 40 %). All the components are weighed and stirred into the beaker to obtain clear mixture solution. The solution is evenly

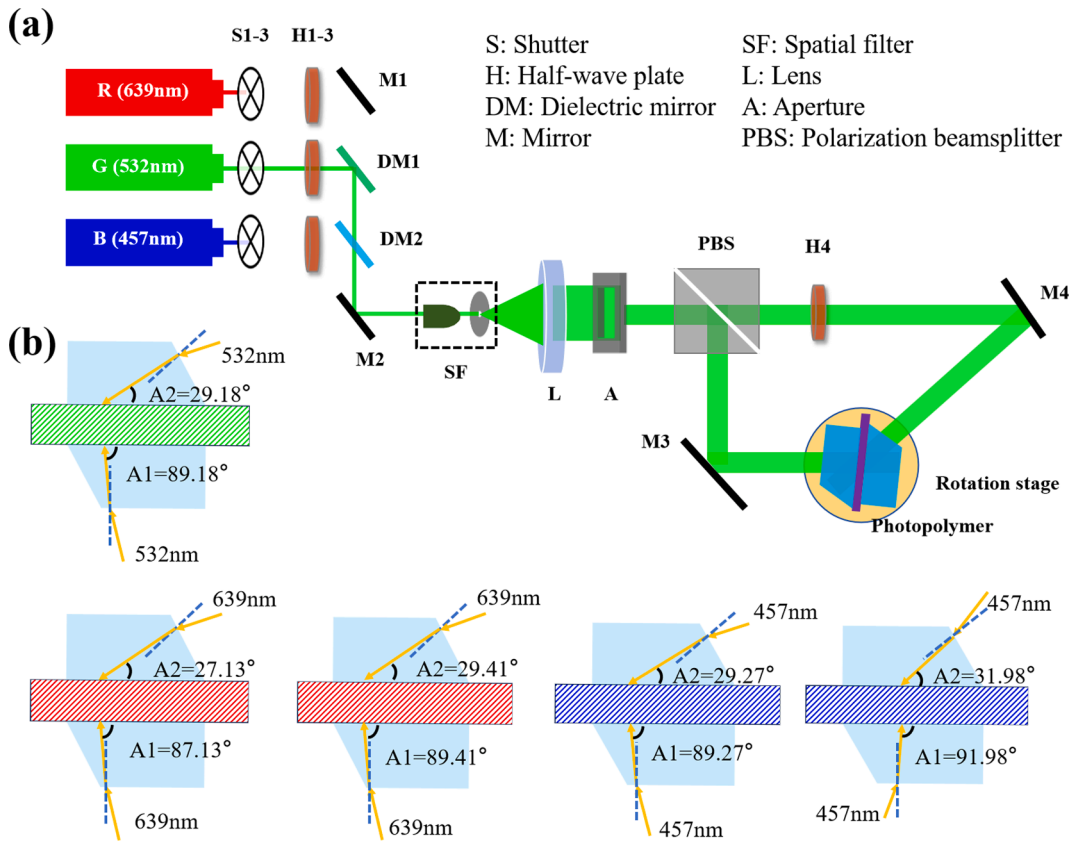

Fig. 5. (a) Optical setup for fabricating the designed RGB VHGs. (b) Exposure angles for RGB VHGs.

coated on clean optical polyethylene terephthalate (PET) or glass substrate by scraper. The dry color sensitive photopolymer films with the thickness of about 15um can be obtained after being placed in the dark room for a period of time. The influence of exposure dosage on the grating diffraction efficiency fabricated with the developed color sensitive photopolymer is investigated. The red, green, and blue gratings all have a grating slanted angle of 30°, with recording wavelengths of 639 nm, 532 nm, and 457 nm. As shown in Fig. 6, when the exposure dosage is less than 10 mJ/cm^2, the diffraction efficiencies of the RGB VHGs are all very low. When the dosage exceeds 10 mJ/cm^2, the diffraction efficiency of green and blue VHGs increases rapidly. The diffraction efficiency of green and blue VHGs would reach the maximum value when the exposure dosages are 30 and 50 mJ/cm^2, respectively.

The photopolymer exhibits lower absorption for long-wavelength light, thus requiring higher exposure dosages to achieve diffraction efficiency for red VHGs. When the exposure dosage is less than 30 mJ/cm^2, the diffraction efficiency increases very slowly. At this time, the exposure is insufficient, so the photopolymer does not fully undergo photochemical reactions, the grating structure is incompletely formed. As the exposure dosage increases from 30 mJ/cm^2 to 100 mJ/cm^2, the diffraction efficiency rapidly rises from approximately 40 % to around 75 %. This is because the exposure dosage reaches the threshold, the photopolymerization and photo-crosslinking reactions within the photopolymer accelerate, the diffraction capability significantly enhances. When the exposure dosage reaches 200 mJ/cm^2, the diffraction efficiency reaches a maximum value of 85 %. Finally, the exposure dosage continues to increase to 250 mJ/cm^2, all the RGB grating diffraction efficiency remains almost unchanged. At this point, the photochemical reaction is approaching saturation, the grating structure tends to be stable, and the diffraction efficiency reaches the upper limit.

The waveguide fabrication process is shown in Fig. 7. The photopolymer solution is uniformly coated on PET transparent optical films using a scraper in the darkroom. After the solvent evaporated completely, the 15 μm thick photopolymer photosensitive films are formed. The photopolymer films are firstly laminated on the glass substrates with refractive index of 1.6, then exposure by RGB lasers with the

Table 3
Exposure parameters for fabricating green VHGs, red and blue stacked VHGs.

Grating	Exposure angle (°)	Wavelength (nm)	Intensity ratio	Exposure intensity (mW/cm^2)	Exposure dosage (mJ/cm^2)
R1	A_1: 87.13 A_2: 27.13	639	Ref : Obj = 1 : 2.12	3.5	200
R2	A_1: 89.41 A_2: 29.41		Ref : Obj = 1 : 1.93	3.7	
G	A_1: 89.18 A_2: 29.18	532	Ref : Obj = 1 : 2.41	5.8	30
B1	A_1: 89.27 A_2: 29.27	457	Ref : Obj = 1 : 2.32	3.8	50
B2	A_1: 91.98 A_2: 31.98		Ref : Obj = 1 : 1.85	4.4	

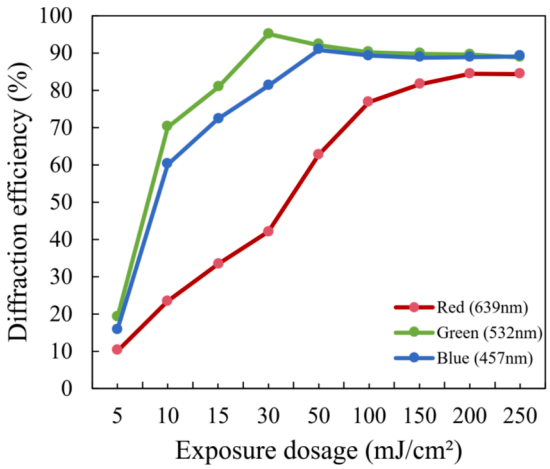

Fig. 6. Diffraction efficiency of RGB VHGs prepared with photopolymer under different exposure dosages.

different interference angles. After the first exposure, the RGB holographic waveguides should be treated by UV curing for 5 min to stabilize the formed grating structure initially. The PET substrate of the first film needs to be peeled off, completing the preliminary preparation of the first grating layer.

After R1 and B1 were completed with UV curing, the diffraction efficiency is not very high, so will not significantly affect the exposure of the second-layer grating R2 and B2. The other photopolymer film is carefully laminated onto the surface of the above prepared grating layer R1 and B1, ensuring close contact without air bubbles. The exposure optical path is then adjusted according to the object-reference light angles of R2 and B2 for the second exposure, followed by another 5-minute UV curing. Subsequently, the PET substrate of the second photopolymer film is also peeled off, leaving the two grating layers tightly attached to the glass substrate. All the prepared waveguides are baked at 110 °C for 10 min at the same time, which would ensure the consistency of diffraction efficiency between the two grating layers as much as possible. This can also enhance the structural stability of the double-layer stacked holographic gratings. Then, the photopolymer film outside the grating regions in the waveguide needs to be removed. Finally, the glue dispenser is used to encapsulate the RGB laminated waveguide, ensuring 50 μm thick air layer between the waveguides to prevent color crosstalk.

2.4. Measurement of the fabricated VHGs

As shown in Fig. 8, we have captured the SEM images for characterizing the surface morphology of the red and blue stacked double-layer grating cross-sections. These images explicitly show key structural characteristics, including the grating period, grating slanted angle, interface between the two grating layers. Compared with Fig. 8(a), the boundary line between the two grating layers B1 and B2 in Fig. 8(b) is tilted by approximately 10°, and this phenomenon is caused by the tilt of the SEM observation angle. On the other hand, when preparing red and green stacked gratings, it is necessary to adjust the interference angle between the object and reference beams. The adjustment of the exposure angle will inevitably lead to differences in slanted angles of the grating fringes, and this could be thoroughly resolved by using a exposure fixture. Specifically, the SEM imaging results verify that the grating periods are generally consistent with the designed values, and that the layer interfaces remain distinct without significant inter diffusion, which is critical for ensuring the independent optical performance of each grating layer.

The ultraviolet–visible spectrophotometer (TU-1901, Persee) is used to test the diffraction efficiency of the fabricated RGB VHGs changed by incident wavelength. As shown in Fig. 9, the variable-angle exposure method is efficient to prepare red and blue stacked VHGs accurately according to the designed values. The red and blue VHGs each have two diffraction peaks at the designed wavelengths of 450 nm, 470 nm, 600 nm and 632 nm. The diffraction efficiencies of the red and blue VHGs reached 62.68 % and 74.24 % respectively. Since the diffraction bandwidth of a single-layer grating is only about 12–15 nm, the diffraction efficiency curves of the laminated red and green VHGs showed an M-shaped distribution.

In addition, the measurement results also proved that the stacked grating structure can effectively expand the diffraction bandwidth of the VHG. The diffraction bandwidth of the blue stacked VHG is expanded to around 40 nm, and the red stacked VHG is also broadened to about 45 nm. Meanwhile, it is found that the efficiency of the first-layer grating in the red and blue stacked VHGs is generally lower than that of the second-layer. This is partly because the first-layer grating is not baked in time after exposure and ultraviolet treatment, and the attached second-layer will partially dissolve the first-layer grating structure. On the other hand, considering the light absorption and scattering by the first grating layer, the exposure intensity and time for the second grating layer could be optimized. If the first layer exhibits higher absorption at the exposure wavelength of the second layer, the exposure intensity of the second

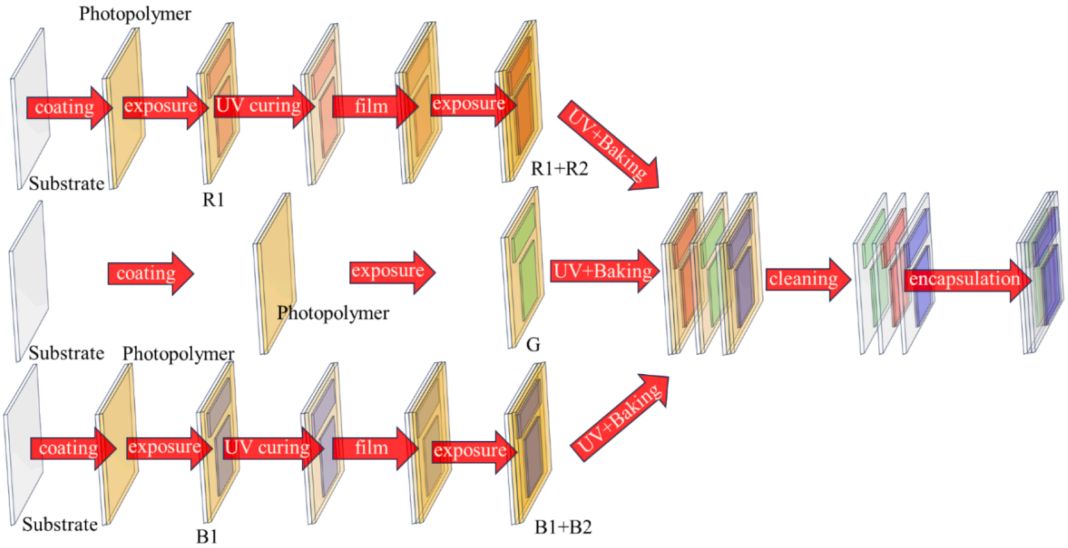

Fig. 7. Preparation process of the chromatic holographic waveguides.

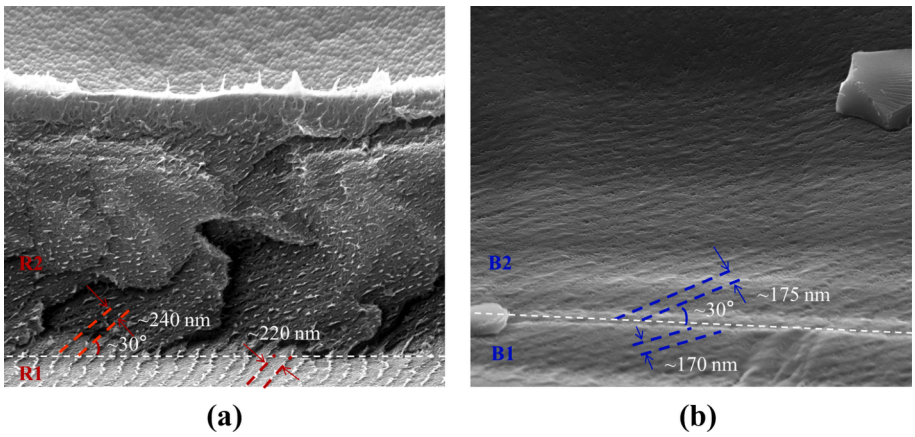

Fig. 8. SEM microscopic structure characterizations. (a) Red double-layer stacked VHGs. (b) Blue double-layer stacked VHGs.

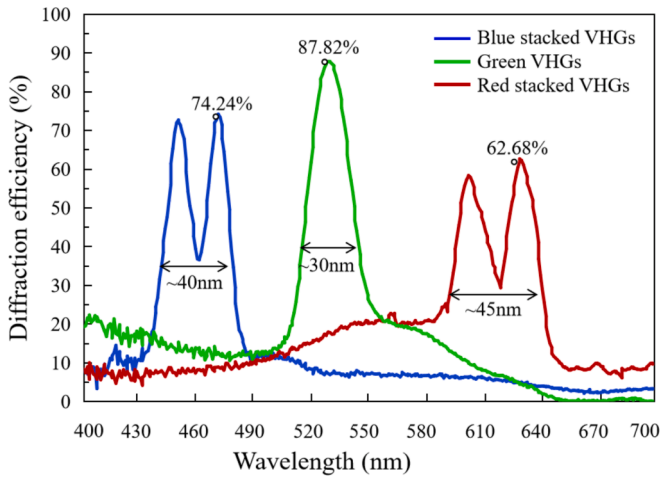

Fig. 9. Measured diffraction efficiency curves of RGB VHGs at different incident wavelengths.

layer should be increased to compensate for the light loss. According to the relationship between exposure dosages and diffraction efficiency for fabricating RGB VHGs illustrated in Fig. 6, we can predict and calculate the required exposure time for the second layer in the stacked structure to match the diffraction efficiency of the first VHG.

By contrast, the peak diffraction efficiency of the green VHG is much higher, nearly approaching to 90 %, with the widest single layered diffraction bandwidth at around 30 nm. The experimental results demonstrate that the fabricated red, green, and blue VHGs all meet the requirements for waveguide coupling, and the actual results align well with the design.

3. Near-eye display prototype

To simultaneously achieve high-brightness, large FOV and full-color waveguide displays, we propose a RGB three-layer waveguide (R1 + R2, G, B1 + B2) to realize full color display, as illustrated in Figs. 10(a) and 10(b). Meanwhile, a double-layer stacked grating structure is adopted to expand the diffraction bandwidth of red and blue VHGs for increasing the display FOV. As shown in Table 4, a detailed comparison is made between the proposed chromatic waveguide display with stacked VHGs in this paper and the previous single-layer and double-layer chromatic

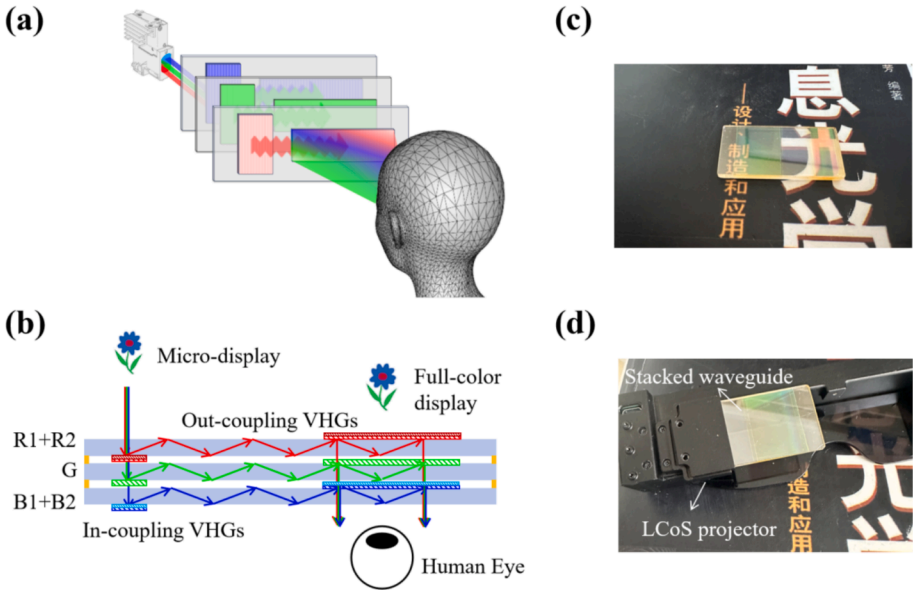

Fig. 10. (a) Schematic diagram of the prototype. (b) Imaging principle of the chromatic holographic waveguides with the double-layer red and blue VHGs. (c) Photos of holographic waveguides. (d) AR near-eye display prototype.

Table 4
Comparison between the previous and our proposed chromatic VHG waveguide displays.

Waveguide configuration	Grating structure	RGB Diffraction efficiency	Crosstalk	FOV
Single layer [22,23]	Composite RGB grating in single layer (R + G + B)	Before optimization: 16 %, 20 %, 10 % ; After optimization: 30 %, 34 %, and 28 %	Exist	Horizontal 17°
	Double grating layer (R, G + B)	40 %, 44 %, 42 %		
	Three grating layer (R, G, B)	10 %, 23 %, 30 %		
Double layer [4]	Layer 1: single layer green VHG; Layer 2: red and blue stacked VHGs	~70 %, ~90 %, ~80 %	Less than 0.2 %	Horizontal 16°
This work	Layer 1: double layer red VHGs Layer 2: single layer green VHG Layer 3: double layer blue VHGs	62.68 %, 87.82 %, 74.24 %	None	Horizontal 24.4° Diagonal 28°

waveguides.

For verifying the imaging capability of the prepared chromatic VHG holographic waveguide, we developed a near-eye display prototype as shown in Figs. 10(c) and 10(d). A clamping structure was designed to fix the three-layered waveguides at the exit pupil position of the LCoS projector, where the in-coupling grating area precisely overlaps. In the out-coupling region of the waveguide, the observers can see the images projected from the LCoS projector.

As illustrated in Figs. 11(a) and 11(c), we used color natural images "parrot" and monochromatic letter "CAB" as input images for the near-eye display prototype. The actual displayed images were captured at the designed view point of the waveguide using a fixed-focus camera. During the capture, the camera was positioned 18 mm away from the out-coupling grating. The final display results are shown in Fig. 11. The displayed images contain full-color information, and the black background in the original image becomes transparent in the displayed virtual image, allowing observers to see the surrounding environment unobstructed through the waveguide.

The actual full-color imaging effect shown in Fig. 11(b) indicates that, due to the highest diffraction efficiency and widest bandwidth of the prepared blue and red stacked VHGs in this paper, the red and blue component has the highest luminance in the displayed image. The imaging results are consistent with the measuring diffraction efficiency curve of the grating. The white balance of the displayed image can be improved by adjusting the ratio of the red, green, and blue channels of the LCoS micro-display. The green screen displayed on the right are slightly dark. This is because the actual diffractive bandwidth of the prepared green VHGs is relatively narrower, compared with red and blue stacked VHGs. This can be improved by further optimizing the RIM of photopolymers.

Also, it is worth noting that the ghost images existed in the actual RGB monochromatic display images, as shown in Fig. 11(d). We found that most ghost images are attributed by the LCoS collimator. The actual output images from the collimator revealed the presence of many ghost images, which is due to the use of beam splitters and spherical mirrors in the LCoS projecting system. If the parallelism between the two beam splitters is not high, some imaging rays are prone to form secondary artifacts near the main image. Additionally, the waveguide would reflect and diffract parts of light beams emitted from the collimator, mainly causing the formation of ghost images. Therefore, in practical applications, it is necessary to apply anti-reflection coatings on the waveguide to reduce ghost images and enhance the display quality.

To quantitatively characterize the imaging performance, this paper also tested display parameters such as luminance and FOV of the prototype, with the measurement methods shown in Figs. 12(a) and 12(b). The prototype to be tested was fixed on the optical platform and adjusted to the standard working state. A whiteboard with scales was placed 10 cm away from the prototype, while the holographic waveguide was kept horizontal with the whiteboard.

After powering and connecting the prototype to the display signal, a camera is used to record the area of the whiteboard scale covered by the maximum display screen. According to the area of the display screen and

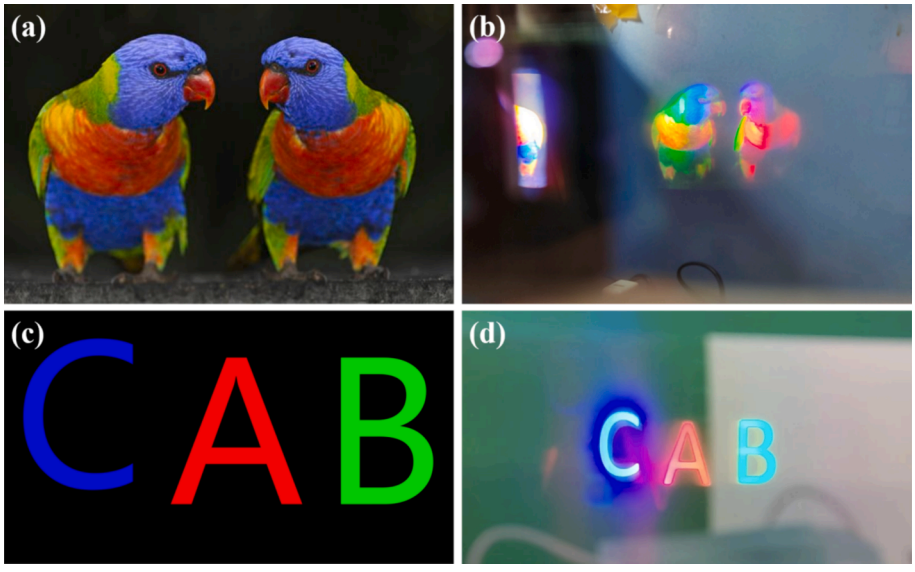

Fig. 11. Actual display results of the near-eye display prototype. (a) Original input full color image "parrot"; (b) Full color imaging results; (c) Monochromatic input image "CAB"; (d) Monochromatic imaging results.

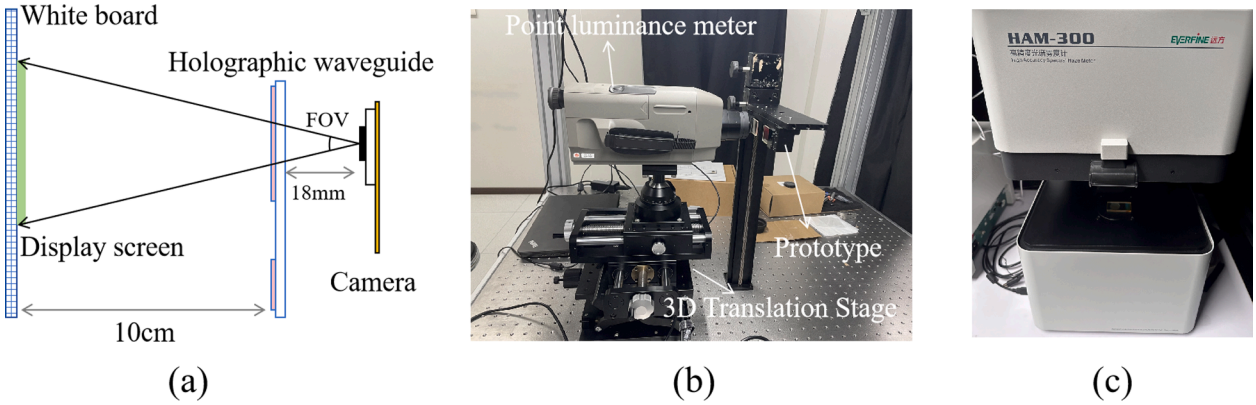

Fig. 12. Measurement methods of the developed near-eye display prototype. (a) FOV. (b) Luminance. (c) Optical transmittance and scattering degree.

the distance from the observation point to the white board, the horizontal FOV is calculated as 24.4°, the vertical FOV was 14°, so the actual displayed diagonal FOV is approximately 28°. Also, the ANSI nine-point method is used to test the luminance of the virtual image displayed by the prototype. Firstly, the luminous flux of the LCoS projection optical engine is tested by the integrating sphere (HAAS-2000, Everfine) to be 2.4 lm. Then, the point luminance meter (CS-200, Konica Minolta) is used to test the luminance of nine points with the self-developed 3D translation stage when displaying a full-white image, and the average value is calculated as 563.8 nit, and the optical imaging efficiency can reach 234.9 nit/lm.

The optical transmittance and scattering degree (haze) of the grating waveguide device are also very important parameters, which affect the clarity of the human eye's view of the surrounding environment. We also employed the visible-infrared spectral haze meter (HAM-300, Everfine) to measure the total optical transmittance and scattering degree of the waveguide's out-coupling area, as illustrated in Fig. 12(c). The measured total optical transmittance and scattering degree are 72.01 % and 1.12 % within the visible wavelength range (380 ~ 780 nm) under D65 light source, respectively.

4. Conclusions

Firstly, we proposed the design methods for 1D EPE holographic waveguide configurations, which realized the diagonal FOV of 28°, ER of 18 mm, eye box of 14 × 10 mm^2. Based on the spectrum of LCoS projector, we designed and fabricated RGB VHGs for waveguide in-coupling and out-coupling. Also, the stacked grating structures were applied for expanding the diffractive bandwidth of red and blue VHGs. The color sensitive acrylate-based photopolymer was utilized for fabricating chromatic VHG waveguides, which variable-angle exposure methods and post preparation process were also introduced and analyzed. The experimental results demonstrated that the corresponding diffraction efficiency of VHGs prepared with the photopolymer all exceed 62 % at the RGB exposure dosage of 200 mJ/cm^2, 30 mJ/cm^2 and 50 mJ/cm^2. The imaging results of the prototype indicated that the fabricated chromatic waveguide meet the requirements for near-eye display, with the optical efficiency of 234.9 nit/lm, luminance of 563.8 nit and high ambient light transmittance of 72 %. Also, stacked grating structure is effectively utilized to expand a diagonal FOV of 28°.

CRediT authorship contribution statement

Zhongwen Shen: Conceptualization, Methodology, Formal analysis, Resources, Writing – original draft, Funding acquisition. **Chao Ping Chen:** Validation, Writing – review & editing, Supervision, Project administration, Funding acquisition. **Zhendong Wu:** Formal analysis, Software, Data curation. **Dawei Zhu:** Validation, Data curation, Funding acquisition. **Yan Yang:** Validation, Supervision, Funding acquisition.

Declaration of competing interest

The authors declare that they have no known competing financial interests or personal relationships that could have appeared to influence the work reported in this paper.

Acknowledgments

This work is supported by Ministry of Industry and Information Technology of China (GO0300164/001), Natural Science Foundation of Chongqing Municipality (cstb2023nscq-msx0465), Natural Science Foundation of Jiangsu Higher Education Institutions of China (22KJD510006), Science and Technology Development Center of Ministry of Education (2023IT048), and Start-up Fund for New Talented Researchers of Nanjing Vocational University of Industry Technology (YK22-02-03, YK21-02-01).

Data availability

Data will be made available on request.

References

[1] Y. Xiong, Z. He, C.P. Chen, X. Li, A. Li, Z. Ye, J. Lu, G. He, Y. Su, Coherent backlight system for flat-panel holographic 3D display, Opt. Commun. 296 (2013) 41–46.
[2] M.G. Moharam, T.K. Gaylord, Rigorous coupled-wave analysis of planar-grating diffraction, J. Opt. Soc. Am. 71 (7) (1981) 811–818.
[3] Y. Ding, Q. Yang, Y. Li, Z. Yang, Z. Wang, H. Liang, S.-T. Wu, Waveguide-based augmented reality displays: perspectives and challenges, eLight 3 (2023) 24.
[4] H. Mukawa, K. Akutsu, I. Matsumura, S. Nakano, T. Yoshida, M. Kuwahara, K. Aiki, A full-color eyewear display using planar waveguides with reflection volume holograms, J. Soc. Inf. Disp. 17 (3) (2009) 185–193.
[5] Z.-H. He, C.-P. Chen, J.-L. Zhu, Y.-C. Yuan, Y. Li, W. Hu, X. Li, H.-J. Li, J.-G. Lu, Y.-K. Su, Electrically tunable holographic polymer templated blue phase liquid crystal grating, Chin. Phys. B 24 (6) (2015) 064203.
[6] Y. Wu, C.P. Chen, L. Zhou, Y. Li, B. Yu, H. Jin, Design of see-through near-eye display for presbyopia, Opt. Express 25 (8) (2017) 8937–8949.
[7] T. Yoshida, K. Tokuyama, Y. Takai, D. Tsukuda, T. Kaneko, N. Suzuki, T. Anzai, A. Yoshikaie, K. Akutsu, A. Machida, A plastic holographic waveguide combiner for light-weight and highly-transparent augmented reality glasses, J. Soc. Info. Disp. 26 (5) (2018) 280–286.
[8] Y. Zhang, X. Zhu, A. Liu, Y. Weng, Z. Shen, B. Wang, Modeling and optimizing the chromatic holographic waveguide display system, Appl. Opt. 58 (34) (2019) G84–G90.
[9] Z. Shen, Y. Zhang, A. Liu, Y. Weng, X. Li, Volume holographic waveguide display with large field of view using a Au-NPs dispersed acrylate-based photopolymer, Opt. Mater. Express 10 (2) (2020) 312–322.
[10] Z. Shen, Y. Weng, Y. Zhang, C. Wang, A. Liu, X. Li, Holographic recording performance of acrylate-based photopolymer under different preparation conditions for waveguide display, Polymers 13 (6) (2021) 936.
[11] C. Wang, Y. Zhang, Y. Weng, Z. Shen, R. Wei, Y. Gu, L. Zhang, Holographic waveguide display with large field of view based on volume holographic grating, J. Soc. Info. Disp. 31 (6) (2023) 433–442.

[12] M. Weng, Y. Wang, X. Ren, Q. Lu, Study on two-dimensional exit pupil expansion for diffractive waveguide based on holographic volume grating, Appl. Sci. 13 (21) (2023) 11858.
[13] M. Murry, I. Naydenova, S. Martin, Review of recent advances in photosensitive polymer materials and requirements for transmission diffractive optical elements for LED light sources, Opt. Mater. Express 13 (12) (2023) 3481–3501.
[14] D. Ni, D. Cheng, Y. Wang, T. Yang, X. Wang, C. Chi, Y. Wang, Design and fabrication method of holographic waveguide near-eye display with 2D eye box expansion, Opt. Express 31 (31) (2023) 11019–11040.
[15] F.-K. Bruder, T. Facke, T. Rolle, The chemistry and physics of Bayfol HX film holographic photopolymer, Polymers 9 (10) (2017) 472.
[16] L. Cao, S. Wu, J. Hao, C. Zhu, Z. He, Z. Zhang, S. Zong, F. Zhang, G. Jin, Enhanced diffraction efficiency of mixed volume gratings with nanorod dopants in polymeric nanocomposite, Appl. Phys. Lett. 111 (2017) 141104.
[17] J. Ma, T. Wu, Y. Cui, J. Li, J. Wang, P. Su, Modified monomer diffusion model for volume holographic grating formation in photopolymers, Appl. Opt. 59 (13) (2020) 3952–3958.
[18] Y. Wu, B. Chrysler, R. Kostuk, Design and fabrication of cascaded dichromate gelatin holographic filters for spectrum-splitting PV systems, J. Photon. Energy 8 (1) (2018) 017001.
[19] Z. Diao, L. Kong, J. Yan, J. Guo, X. Liu, L. Xuan, L. Yu, Electrically tunable holographic waveguide display based on holographic polymer dispersed liquid crystal grating, Chin. Opt. Lett. 17 (1) (2019) 012301.
[20] S.B. Odinokov, M.V. Shishova, V.V. Markin, D.S. Lushnikov, A.Y. Zherdev, A. B. Solomashenko, D.V. Kuzmin, N.V. Nikonorov, S.A. Ivanov, Augmented reality display based on photo-thermo-refractive glass planar waveguide, Opt. Express 28 (12) (2020) 17581–17594.
[21] M.V. Shishova, S.B. Odinokov, A.Y. Zherdev, D.S. Lushnikov, Recording of multiplexed volume gratings via a phase mask for augmented reality waveguides, Appl. Opt. 60 (4) (2021) A140–A144.
[22] J.-A. Piao, G. Li, M.-L. Piao, N. Kim, Full color holographic optical element fabrication for waveguide-type head mounted display using photopolymer, J. Opt. Soc. Korea 17 (3) (2013) 242–248.
[23] M.-L. Piao, N. Kim, Achieving high levels of color uniformity and optical efficiency for a wedge-shaped waveguide head-mounted display using a photopolymer, Appl. Opt. 53 (10) (2014) 2180–2186.
[24] R. Shi, J. Liu, H. Zhao, Z. Wu, Y. Liu, Y. Hu, Y. Chen, J. Xie, Y. Wang, Chromatic dispersion correction in planar waveguide using one-layer volume holograms based on three-step exposure, Appl. Opt. 51 (20) (2012) 4703–4708.
[25] Z. Wu, J. Liu, Y. Wang, A high-efficiency holographic waveguide display system with a prism in-coupler, J. Soc. Info. Disp. 21 (12) (2013) 524–528.
[26] N. Zhang, J. Liu, J. Han, X. Li, F. Yang, X. Wang, B. Hu, Y. Wang, Improved holographic waveguide display system, Appl. Opt. 54 (12) (2015) 3645–3649.
[27] C. Yu, Y. Peng, Q. Zhao, H. Li, X. Liu, Highly efficient waveguide display with space-variant volume holographic gratings, Appl. Opt. 56 (34) (2017) 9390–9397.
[28] J. Han, J. Liu, X. Yao, Y. Wang, Portable waveguide display system with a large field of view by integrating freeform elements and volume holograms, Opt. Express 23 (3) (2015) 3534–3549.
[29] X. Shi, J. Liu, J. Xiao, J. Han, Design of a compact waveguide eyeglass with high efficiency by joining freeform surfaces and volume holographic gratings, J. Opt. Soc. Am. A 38 (2) (2021) A19–A26.
[30] C.P. Chen, L. Mi, W. Zhang, J. Ye, G. Li, Waveguide-based near-eye display with dual-channel exit pupil expander, Displays 67 (2021) 101998.
[31] C.P. Chen, L. Mi, W. Zhang, J. Ye, G. Li, Wide-field-of-view near-eye display with dual-channel waveguide, Photonics 8 (12) (2021) 557.
[32] C.P. Chen, Y. Cui, Y. Chen, S. Meng, Y. Sun, C. Mao, Q. Chu, Near-eye display with a triple-channel waveguide for metaverse, Opt. Express 30 (17) (2022) 31256–31266.
[33] C.P. Chen, X. Ma, S.P. Zou, T. Liu, Q. Chu, H. Hu, Y. Cui, Quad-channel waveguide based near-eye display for metaverse, Displays 81 (2023) 102582.
[34] C.P. Chen, X. Wu, J. Wang, B. Han, Y. Y, S. Liu, Penta-channel waveguide-based near-eye display with two-dimensional pupil expansion, Displays 88 (2025) 102999.
[35] Q. Feng, J. Cai, Y. Guo, M. Guo, Z. Wang, G. Lv, Genetic-algorithm-based waveguide display system with a multiplexed volume holographic grating, Appl. Opt. 63 (8) (2024) 2070–2077.
[36] R. Kaur, B. Das, J.H. Park, R. Kumar, Improved color uniformity in monochrome holographic waveguide based near eye displays, Opt. Express 33 (11) (2025) 22255–22269.
[37] P. Liu, C. Luo, T. Lee, G. Nero, T. Zhang, Y. Pei, X. Deng, Y. Takashima, Expanding field-of-view of near-to-eye display by hybrid angular and wavelength multiplexing, Opt. Express 33 (1) (2025) 1466–1477.